

# ULRR

## Experimental characterization of novel microdiffuser elements

Item Type	Meetings and Proceedings
Authors	Ehrlich, Leicester;Punch, Jeff;Jeffers, Nicholas;Stafford, Jason
Citation	Journal of Physics: Conference Series;525, 012008
Publisher	IOP Publishing
Download date	2026-06-06 17:00:44
Item License	<a href="https://creativecommons.org/licenses/by-nc-sa/1.0/">https://creativecommons.org/licenses/by-nc-sa/1.0/</a>
Link to Item	<a href="https://hdl.handle.net/10344/6499">https://hdl.handle.net/10344/6499</a>

## Experimental characterization of novel microdiffuser elements

L Ehrlich<sup>1</sup>, J Punch<sup>1</sup>, N Jeffers<sup>2</sup> and J Stafford<sup>2</sup>

<sup>1</sup>CTVR, Stokes Institute, University of Limerick, Limerick, Ireland

<sup>2</sup>Bell Labs Ireland, Thermal Management Research Group, Alcatel-Lucent, Dublin, Ireland

E-mail: leicester.ehrlich@ul.ie

**Abstract.** Micropumps can play a significant role in thermal management applications, as a component of microfluidic cooling systems. For next-generation high density optical communication systems, in particular, heat flux levels are sufficiently high to require a microfluidic circuit for cooling. Valveless piezoelectrically-actuated micropumps are a particularly promising technology to be deployed for this application. These pumps exploit the asymmetric flow behaviour of microdiffusers to achieve net flow. They feature no rotating or contacting parts, which make them intrinsically reliable in comparison to micropumps with active valves. In this paper, two novel microdiffuser elements are reported and characterized. The micropumps were fabricated using a 3D Printer. Each single diffuser had a length of 1800  $\mu\text{m}$  and a depth of 400  $\mu\text{m}$ . An experimental characterization was conducted in which the flow rate and differential pressure were measured as a function of operating frequency. In comparison with standard diffuser, both elements showed an increase in differential pressure in the range of 40 – 280 %, but only one of the elements exhibited an improved flow rate, of about 85 %.

### 1. Introduction

Next generation high density Photonic Integrated Circuits (PICs) show significant advantages in terms of performance, miniaturisation and energy efficiency. However the thermal management of these devices is extremely challenging. Especially, the integrated laser arrays produce high heat fluxes over  $10^2 \text{ W/cm}^2$  and furthermore require tight operating temperature limits of about  $\pm 0.1 \text{ K}$ . Thermoelectric modules (TEMs) are currently used to achieve thermal control, but these are limited in terms of heat flux to about  $10^1 \text{ W/cm}^2$  and are notably inefficient in comparison with conventional vapour phase refrigeration. To overcome this thermal issue for future generation PICs, a microfluidic circuit for cooling individual devices is needed. Micropumps play a significant role for thermal control and are essential for running a microfluidic cooling system. However, these pumps have to fulfil several requirements such as a long lifetime, easy maintenance, low cost and miniature structure [1]. As valveless piezoelectric actuated micropumps feature no rotating or contacting parts (high reliability) and have a simple structure, they are a particularly promising technology to be deployed for this application. These pumps exploit the asymmetric flow behaviour of microdiffusers to achieve net flow. As the flow in artefacts such as microchannels and microgaps require high pressure heads [2], an



enhancement of the performance of these pumps is needed to fulfil the requirements needed for the cooling of next generation PICs.

In recent years, different configurations of micropumps have been developed and studied, however piezoelectrically-actuated micropumps are the most reported and deployed. The advantages of piezoelectric actuation are a relatively high displacement, force and fast mechanical response as well as high flow rates per unit area, compared to other actuation methods [3]. The pumping action of piezoelectrically-actuated pumps can be divided into two modes, as illustrated in Fig. 1. During the supply mode, the volume of the pumping chamber increases as the piezoelectric element moves upwards. This causes a decrease of pressure inside the pumping chamber which forces the fluid to flow into the chamber through the inlet. During the pumping mode, the pressure increases inside the chamber due to the downward movement of the piezoelectric element, pushing the fluid through the outlet. For this mechanism to achieve a positive fluid displacement, valves at the inlet and outlet must be employed.

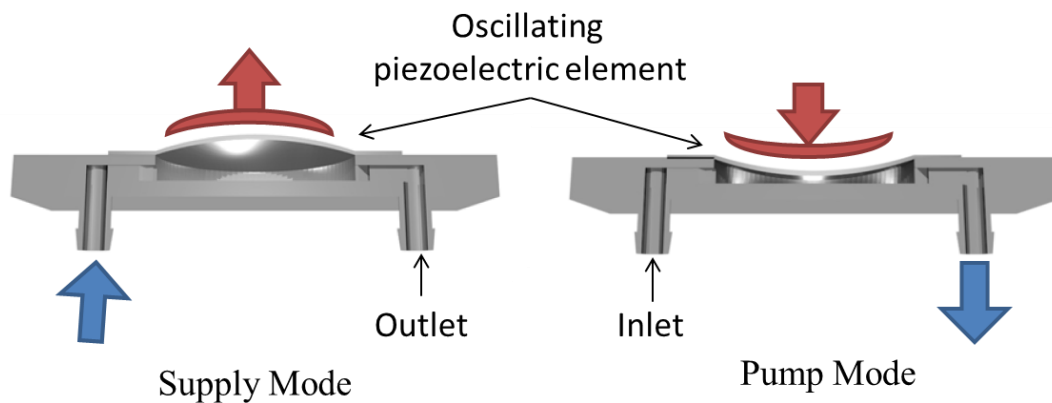


**Figure 1.** Operation of piezoelectrically-actuated micropump

Commercially available valveless micropumps use standard diffuser/nozzle elements to bias the flow. Several studies have been undertaken to optimize the standard diffuser/nozzle element [4-5]. However, these studies mainly concentrated on the effect of different design parameters such as diffuser angle and length. In this study, two novel diffuser elements are presented with the intention to improve the performance compared to the standard diffuser/nozzle element. The novel elements employ protrusions inside the diffuser chamber as well as side channels to reduce the backflow and consequently to increase the efficiency of the diffuser element. The micropumps were manufactured using 3D printing methods. A 3D printer uses an additive process, in which successive layers of a specific material are laid down to create the intended shape. Differential pressure and flow rate were measured for a range of operating frequencies to characterize the micropump design and experimentally assess the diffuser elements. For the two novel diffuser elements, a differential pressure improvement was achieved in the range 40 – 280 % compared to the standard diffuser/nozzle element. A net flow rate improvement of about 85 % was achieved with only one of the novel diffuser elements.

## 2. Novel Microdiffuser Elements

One important component responsible for the performance of piezoelectrically-actuated micropumps are the microdiffuser elements located at the inlet and outlet. As mentioned before, several studies have been undertaken to investigate the effects of geometrical parameters in standard diffuser/nozzle elements. In this study, however, the performance of a piezoelectrically-actuated micropump is

intended to be enhanced by adding channels and protrusions inside the diffuser chamber to reduce the backflow during supply mode. The length and height of the investigated microdiffuser were set to  $1800\ \mu\text{m}$  and  $400\ \mu\text{m}$ , respectively. These dimensions were based on the dimensions published by Sun et al. [6]. The effects of different diffuser lengths and widths were not investigated as the purpose of this study was to characterize the effects of the additional channels and protrusions inside the diffuser chamber. The two novel diffuser elements, along with the standard diffuser/nozzle element, are shown in Fig. 2.

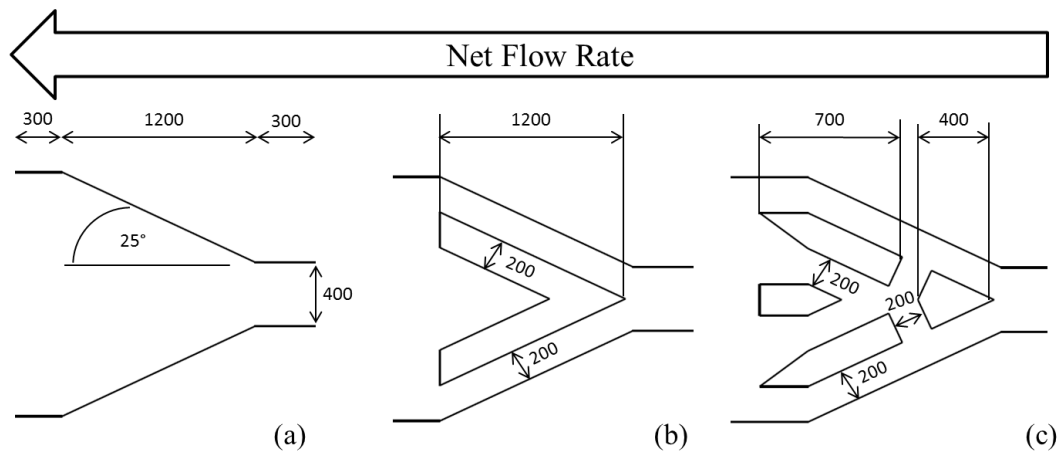


**Figure 2.** Microdiffuser elements (a) diffuser/nozzle, (b) V-shaped, (c) X-shaped (dimensions in  $\mu\text{m}$ )

The inlet width, length and height of the diffuser were set to  $400\ \mu\text{m}$ ,  $1800\ \mu\text{m}$  and  $400\ \mu\text{m}$  respectively. All three diffusers had the same outline dimensions (illustrated in Fig.2(a)). The first novel element (V-shaped diffuser Fig.2(b)) featured a V-shaped protrusion in the centre of the diffuser. The protrusion width was set to  $200\ \mu\text{m}$ . During supply mode, it is anticipated that the fluid will be trapped in the V-shaped pocket, reducing the backflow and increasing the efficiency of the diffuser. The second novel element (X-shaped diffuser Fig.2(c)) has four protrusions located inside the diffuser. During pumping mode, the fluid is mainly expected to flow along the two channels located at the edge of the diffuser. During supply mode, however, the flow is anticipated to split into four different flows. The two flow paths in the centre are directed so that they join the two flow paths close to the walls perpendicularly. The convergence of the two flows is postulated to create vortices leading to a reduction in velocity and a reduction of the overall backflow.

### 3. Evaluation of 3D Printed Channels and Protrusions

3D printing is showing promising benefits to be used in the future as a cost-effective alternative to conventional silicon micromachining. Although the accuracies of 3D printers rapidly increased in the last few years, printed parts in the micro scale can still show defects or blockages, especially with the Pro Jet HD 3000 Plus 3D printer used in this study. Consequently, an optical analysis was performed to determine the minimum feature sizes that the 3D printer was capable of printing for a functional diffuser. For printing the material EX 200 from 3D Systems was used. The desired height of the diffusers was fixed to  $400\ \mu\text{m}$ . To this end, several single protrusions and channels with different dimensions were printed. Each protrusion and channel to be investigated was printed five times. The protrusion widths were varied from  $40$  to  $480\ \mu\text{m}$ , and the channel widths were varied from  $100$  to  $800\ \mu\text{m}$ . Each protrusion and channel was printed inline and spanwise to see if any differences in accuracy appeared. (The term inline means that the printed layers are laid down along the orientation of the protrusion or channel; spanwise means the layers are laid down tangential to the orientation of the protrusion or channel). The single channels and protrusions were examined under a Keyence VHX

Digital Microscope. From the recorded 2D images, the area, height and width were measured with the included software. The measured heights for different widths protrusions and channels are shown in Fig. 3.

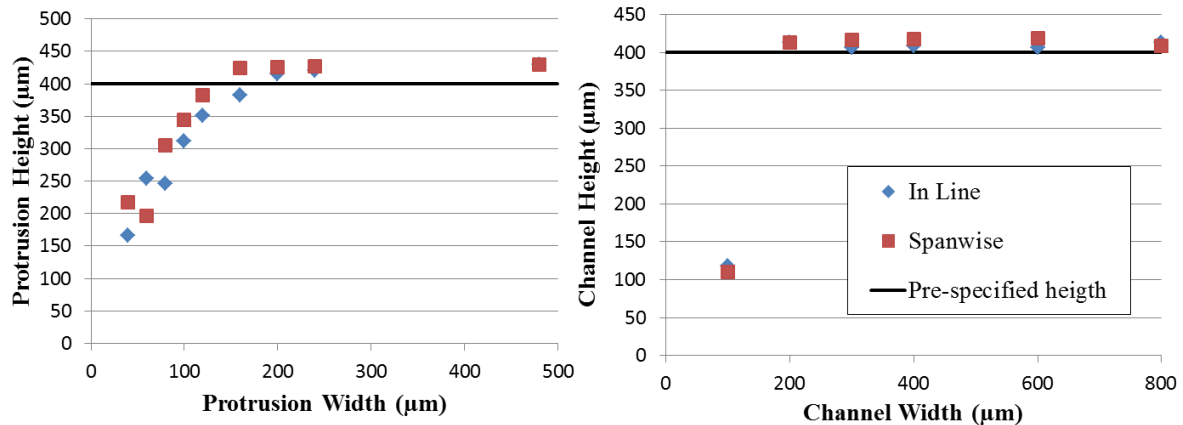


**Figure 3.** Measured protrusion and channel heights for different widths

It can be seen that the desired height of 400 μm for the protrusions (pre-specified height of the diffusers) is reached at a protrusion width of 200 μm. No significant difference between inline and spanwise printing was observed. The results for the channels show a similar outcome: the desired height of 400 μm was also reached at a channel width of 200 μm for both inline and spanwise printing. Based on these results, the dimensions of all protrusions, openings and distances between the two printed parts were set to be greater than 200 μm. Fig. 4 shows, in extracts, the profiles of channels and protrusions for different widths.

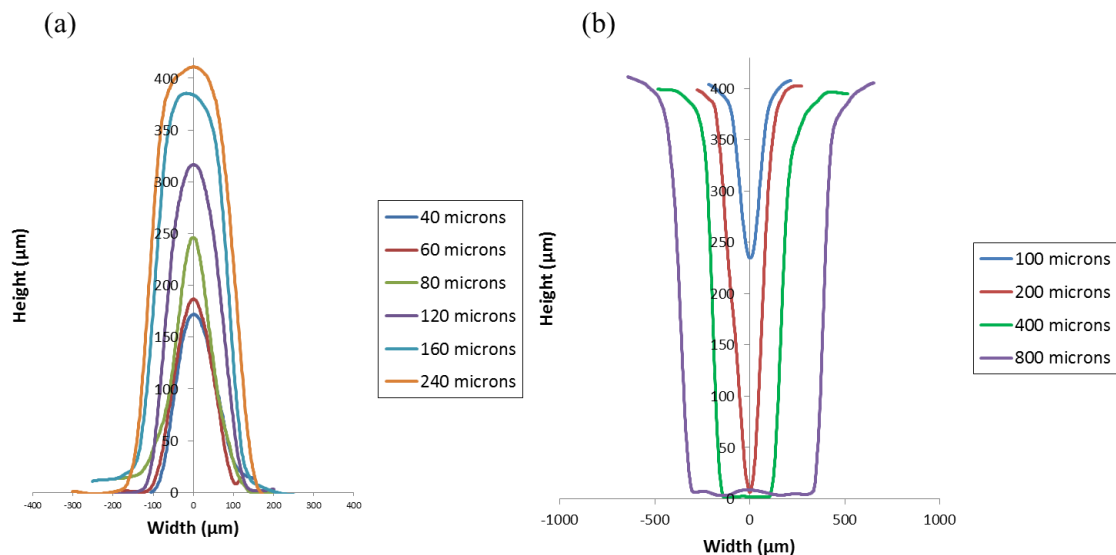


**Figure 4.** Measured profiles: (a) protrusions, (b) channels

It can be seen the bigger the width, the more rectangular (anticipated shape) the channel and protrusion becomes. For the diffuser elements, an inlet width of 400 μm was chosen (described in section 2) as profiles showed almost complete rectangular structure. The protrusion width was set to 200 μm. Microscope images of the two 3D printed novel diffuser elements are shown in Fig. 5. The

images show that the diffusers were printed with neither defects nor blockages, and that their functionality was ensured.

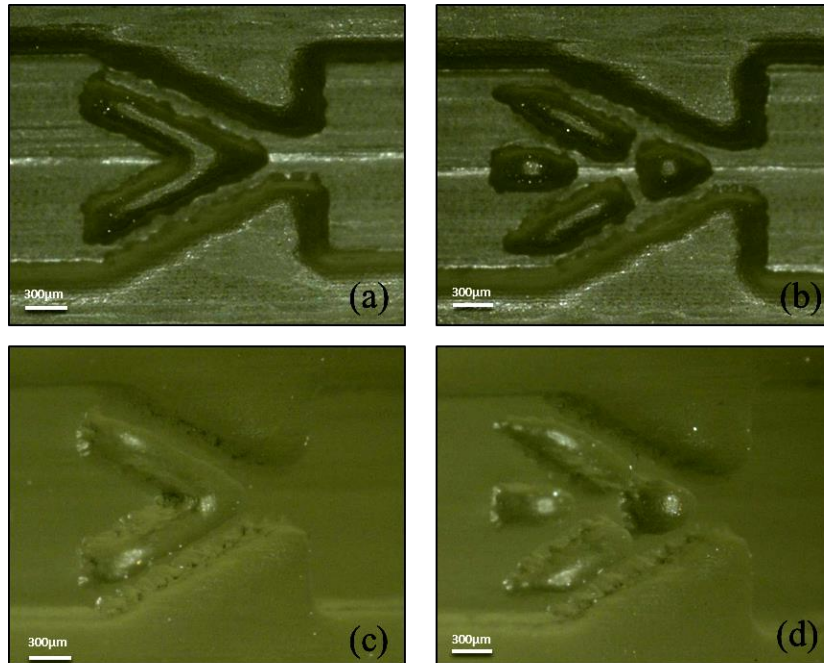


**Figure 5.** Microscope image: (a) V-shaped, (b) X-shaped; angular microscope image: (c) V-shaped, (d) X-shaped

#### 4. Micropump Design and Experimental Set Up

The design of the piezoelectrically-actuated micropumps and the experimental set up for characterization is discussed in section 4.1 and section 4.2 respectively. Section 4.3 describes the uncertainties in the experimental set up for characterization of the micropumps.

##### 4.1. Micropump Design

The micropump assembly was manufactured using the material EX 200 on the Pro Jet HD 3000 Plus 3D printer (same as described in previous section) and is seen in Fig. 6.

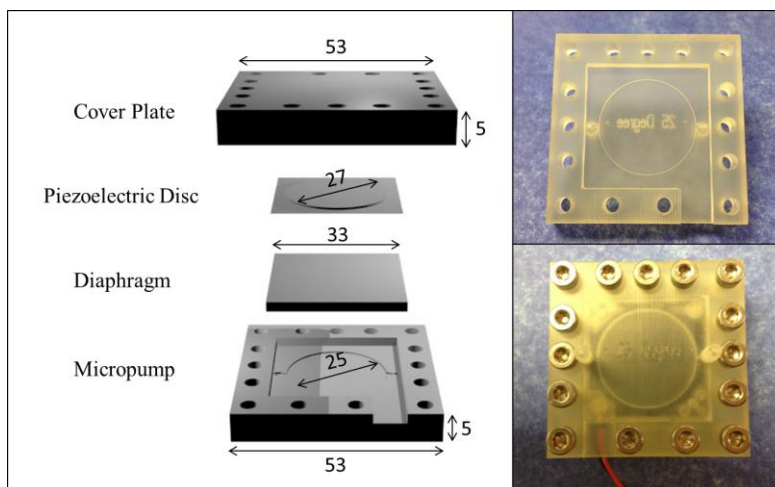


**Figure 6.** (a) exploded view of micropump assembly (dimensions in mm), (b) 3D printed micropump, (c) fully assembled 3D printed micropump

The pumping chamber had a diameter of 25 mm and a height of 400  $\mu\text{m}$ . A steel sheet with a thickness of 200  $\mu\text{m}$  was used as a diaphragm. For actuation, a piezoelectric element from Radionics (Part Number: 724-3162) was employed. The piezoelectric element had a diameter of 27 mm, thickness of 520  $\mu\text{m}$  and was attached to the diaphragm using double-sided adhesive tape. The diaphragm with the attached piezoelectric element was then clamped on top of the pumping chamber and diffuser elements. Clamping was achieved by using fifteen M4 screws with a force sufficiently high to seal the pumping chamber.

#### 4.2. Experimental Set Up

The experimental set up is illustrated in Fig. 7. For the differential pressure measurements, a PX409-015DWUV pressure transducer from Omega was used. The transducer was pre-calibrated and certified by the manufacturer. The flow rate was determined using the DUAL-NE-1000X syringe pump from New Era Pump Systems Inc. To drive the piezoelectric element, a TTI TG2000-20MHz DDS function generator was used to input a sine wave to a Piezo System Inc. EPA-104 power amplifier. Stainless steel Swagelok T-fittings and straight fittings were utilized and flexible vinyl tubing (ID 3.175 mm) was used to couple the experimental components together.

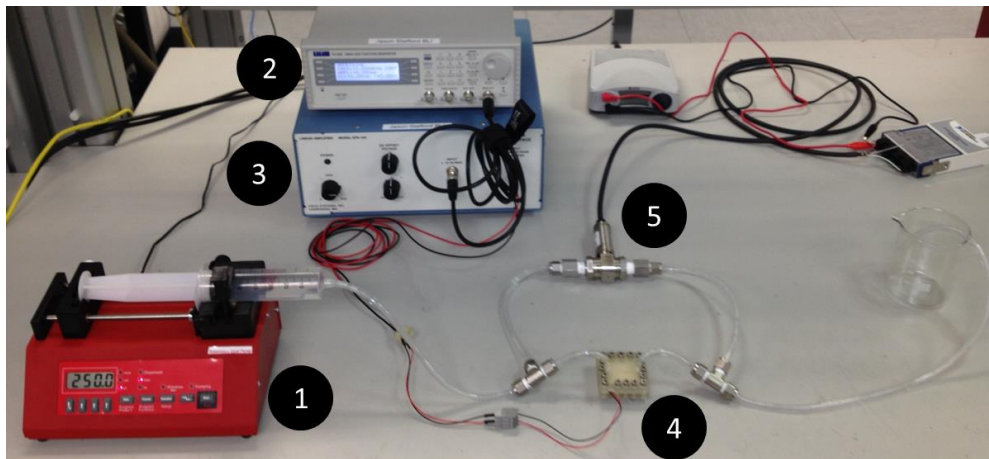


**Figure 7.** Experimental Set Up: 1) Syringe Pump, 2) Function Generator, 3) Power Amplifier, 4) Micropump, 5) Pressure Transducer

Water was used as the working fluid for the experiments. The voltage for driving the piezoelectric element was fixed to 170 V and the frequency was increased between 0 – 100 Hz in 10 Hz steps. Above 100 Hz, the steps were increased to 25 Hz. For every characterization, the frequency was increased until the differential pressure and flow rate went back to zero. For each investigated frequency, the differential pressure was recorded when the system reached a steady state condition. During the differential pressure measurements, the syringe pump was turned off in order to ensure zero flow rate in the system. When the micropump was powered with zero flow in the system, the maximum achievable differential pressure for the given frequency was measured directly at the ports of the pressure transducer.

After a consistent differential pressure was recorded, the syringe pump was turned on with a flow rate of 10  $\mu\text{l}/\text{min}$ . The flow rate was then slowly increased in 10  $\mu\text{l}/\text{min}$  steps. After every increasing step in flow rate, the system was given sufficient time to stabilize. With increasing flow rate of the syringe pump, the differential pressure reduced at the pressure ports as the system gets gradually opened. At a specific flow rate of the syringe pump (system completely open), the differential pressure returned to zero. The flow rate at which the differential pressure was zero corresponds to the maximum flow rate of the micropump at the specified operating frequency.

This differential pressure and net flow rate measurement procedure was conducted for every investigated frequency.

#### 4.3. Experimental Uncertainty

The pressure transducer used in the experimental testing had a range of 100 kPa. This range was chosen as maximum differential pressures of 30 – 50 kPa were anticipated. The total uncertainty of the pressure transducer was given as  $\pm 0.08\%$  over the full scale. However, lower differential pressures were recorded during testing which lead to higher percentage uncertainties than expected. The maximum recorded differential pressures of the three diffuser elements varied between 0.169 – 0.658 % over the full scale of the transducer. As the differences in the measured differential pressures of the diffuser elements were quite high ( $\sim 0.489\%$  between diffuser/nozzle and X-shaped), the transducer was assumed to be accurate enough to show if a performance improvement was achieved with the novel elements.

The syringe pump used for the net flow rate measurement had an uncertainty of  $\pm 1\%$  over the dispensing range, which was sufficiently accurate to record the maximum flow rates (in the range of 6 – 16 % of the dispensing range).

### 5. Results and Discussion

The flow rate measurements and differential pressure measurements are discussed in section 5.1 and 5.2 respectively

#### 5.1. Differential Pressure Measurement

Fig. 8 shows the results of the differential pressure measurements for the three diffuser elements as a function of frequency.

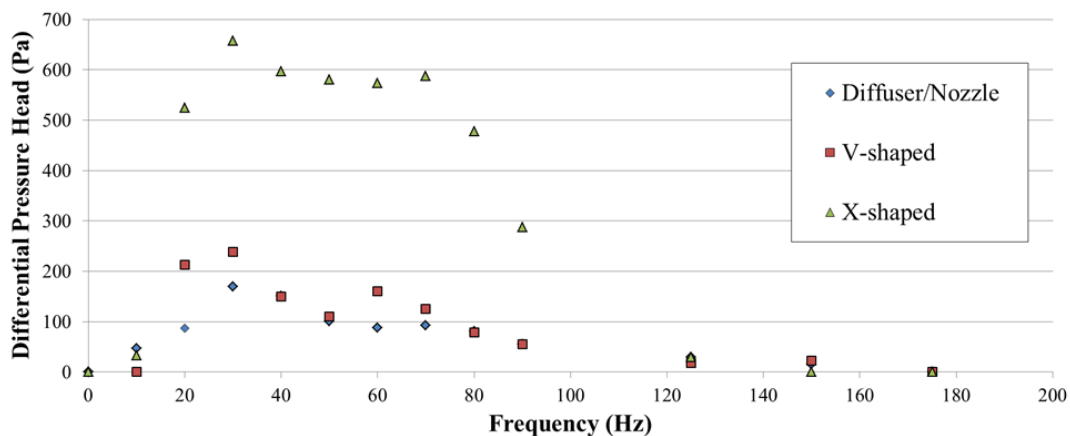


**Figure 8.** Maximum differential pressure as a function of frequency

All three diffuser elements achieve their maximum differential pressure at 30 Hz and, at the highest frequency, of 175 Hz, the differential pressure reverts to zero for all diffuser elements. It was anticipated, however, that the different diffuser elements would reach their maxima at different frequencies. This indicates that the assembly of the piezoelectric element and diaphragm shows inferior peak differential pressure. The lower the displacement of the piezoelectric element, the lower the pressure produced inside the pumping chamber, leading automatically to a reduction of the differential pressure. Higher differential pressures for all three diffuser elements would most likely be achieved with an improved piezoelectric element and a diaphragm with lower damping effects. Most

importantly, however, both novel diffuser elements show an increase in their maximum differential pressure in comparison with the standard diffuser/nozzle element. The V-shaped diffuser shows an increase of the maximum differential pressure of 70 Pa. Although this is within the range of the uncertainty of the pressure transducer, the V-shaped element is most likely to achieve superior differential pressures. Higher values are also obtained between 20 and 40 Hz, as well as between 50 and 80 Hz. Between 40 and 50 Hz and above 80 Hz, however, the V-shaped diffuser element shows similar values to the diffuser/nozzle element. To verify the improved performance of the V-shaped element, measurements with a more accurate pressure transducer are required. The X-shaped diffuser shows an increase of the maximum differential pressure of 489 Pa compared to the diffuser/nozzle element, which is an increase of approximately 280 %. In addition, the X-shaped diffuser shows almost four times the differential pressure values of the diffuser/nozzle element over the whole frequency range of 175 Hz. Even allowing for the uncertainty in the pressure transducer, a significant improvement in differential pressure is achieved with the X-shaped element.

### 5.2. Flow Rate Measurement

Fig. 9 shows the results for the flow rate measurement of the three diffusers for different frequencies at zero differential pressure.

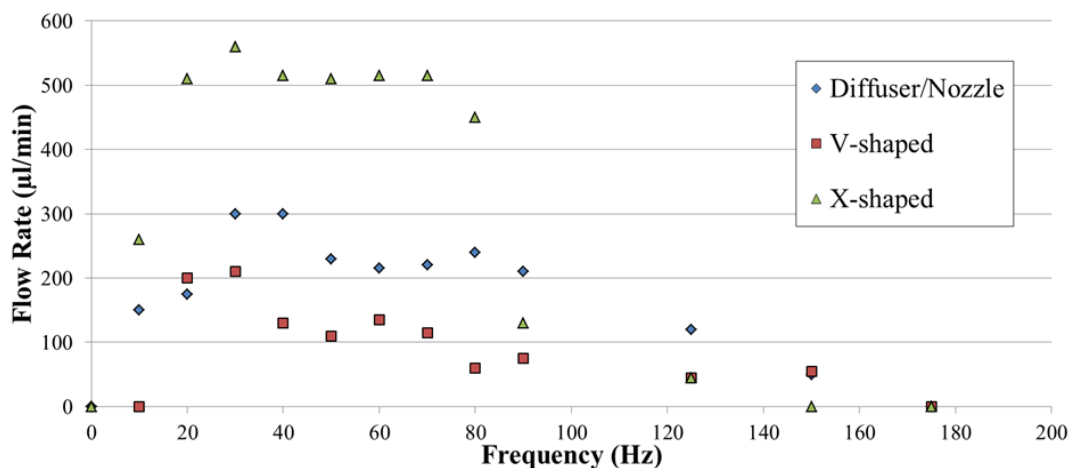


**Figure 9.** Measured net flow rates as a function of frequency

The results of the flow measurement reflect the results for the differential pressure characterization. As all discussed phenomena in the differential pressure measurement section are relevant for the flow rate measurements, only distinct features will be discussed in this sub-section. The diffuser/nozzle element reaches its maximum flow rate of 300  $\mu\text{l}/\text{min}$  at 30 Hz. This trend in the flow rate is as expected from the differential pressure measurements, and it is similar to the behaviour of diffuser/nozzle elements investigated by other authors [7-9]. Although the V-shaped diffuser element shows an increase in the differential pressure, the achieved flow rates are lower over the frequency range than those of the diffuser/nozzle element. This reduction in flow rate occurs as the V-shaped diffuser element has a high flow resistance in the diffuser direction, leading to smaller flow rates during pumping mode than for the diffuser/nozzle element. In the nozzle direction and during supply mode, however, the flow resistance of the V-shaped protrusion is even higher, which reduces the backflow significantly. This results in a low flow rate – high pressure rise pump characteristic. The maximum net flow rate is measured to be 210  $\mu\text{l}/\text{min}$  at 30 Hz. This is 90  $\mu\text{l}/\text{min}$  lower than the maximum value for the diffuser/nozzle element. Similar to the differential pressure measurements, the X-shaped diffuser shows a large increase in the flow rate compared to the diffuser/nozzle element. It reaches its maximum of 560  $\mu\text{l}/\text{min}$  at 30 Hz, about twice the value of the standard diffuser/nozzle element. The flow rate increase indicates that the backflow gets reduced significantly by this element. However, the measured

results do not prove if this is caused by the anticipated vortex areas, or by a much higher flow resistance in the nozzle direction.

## 6. Conclusion

This paper presents the characterization of 3D printed valveless piezoelectrically-actuated micropumps with novel microdiffuser elements. As microchannel cooling requires high pressure heads and high flow rates, the novel X-shaped microdiffuser shows promising results to be used for the application of next generation PICs cooling. With the presented design, the backflow during supply mode was successfully reduced leading to a maximum reached differential pressure of 658 Pa and a maximum flow rate of 560  $\mu\text{l}/\text{min}$ , both at an operating frequency of 30 Hz. This is an improvement of 280% in differential pressure and 85% in net flow rate compared to the standard diffuser/nozzle element. A secondary outcome of this work is the successful demonstration of 3D printing as a fabrication technique for a microfluidic component. Although 3D printing still shows limitations concerning manufacturing in the micro scale, with the rapid increase in technological advances this quite young manufacturing technique will very likely play an important part in the future of microfluidics. For further enhancement of the introduced microdiffuser elements, a numerical optimization of the protrusions and channels will be conducted. A re-characterization of the micropumps with a pressure transducer with higher accuracies is expected to confirm the performance improvement, especially for the V-shaped element.

## Acknowledgement

The authors acknowledge the financial support of Science Foundation Ireland under Grant No. 10/CE/11853. Bell Labs Ireland would like to thank the Industrial Development Authority (IDA) for the continued support.

## References

- [1] Singhal V., Garimella S. V., Raman A., "Microscale pumping technologies for microchannel cooling systems", *Appl Mech Rev* vol 57, no 3, pp 191-248, (2004). More references
- [2] Garimella S.V. and Sobhan C.B., "Transport in microchannels: A critical review", *Annu. Rev. Heat Transfer* 15, pp. 1–50, (2003).
- [3] Iverson B, Garimella S, "Recent advances in microscale pumping technologies: a review and evaluation", *Microfluid Nanofluid*, pp 145-174, (2008).
- [4] Sun C, Yang Z, "Effects of the half angle on the flow rectification of a microdiffuser", *J Micromech Microeng* 17:2031–2038, (2007).
- [5] Nabavi M, Mongeau L, "Numerical analysis of high frequency pulsating flows through a diffuser-nozzle element in valveless acoustic micropumps". *Microfluid Nanofluid*, pp 659-681, (2009).
- [6] Sun C. L., Huang K. H., "Numerical characterization of the flow rectification of dynamic microdiffusers", *Journal of Micromechanics and Microengineering*, pp 1331-1339, (2006).
- [7] Izzo I., Accoto D., Menciassi A., Schmitt L., Dario P., "Modeling and experimental validation of a piezoelectric micropump with novel no moving part valves", *Sensors and Actuators A* 133, pp 128-140, (2007).
- [8] Chandika S., Asokan R., Vijayakuma K.C.K., "Flow characteristics of the diffuser/nozzle micropump – A state space approach", *Flow Measurement and Instrumentation*, pp 28-34, (2012).
- [9] Choi A., Vatanabe S. L., Lima C., Silva E., "Computational and experimental characterization of a low-cost piezoelectric valveless diaphragm pump", *Journal of Intelligent Materials and Structures* 23(1), pp 53-63, (2011).